Measurement of granular entropy

Sean McNamara, Patrick Richard, Sébastien Kiesgen de Richter, Gérard Le Caër, and Renaud Delannay
Institut de Physique de Rennes, UMR UR1-CNRS 6251, Université de Rennes I, Bât. 11A, 35042 Rennes Cedex, France
(Received 13 May 2009; published 10 September 2009)

Recently, Dean and Lefèvre [Phys. Rev. Lett. **90**, 198301 (2003)] developed a method for testing the statistical mechanical theory of granular packings proposed by Edwards and co-workers [Physica A **157**, 1080 (1989); Phys. Rev. E **58**, 4758 (1998)]. The method relies on the prediction that the ratio of two overlapping volume histograms should be exponential in volume. We extend the method by showing that one can also calculate the entropy of the packing and also that the method can yield false positive results when the histograms are Gaussians with nearly identical variances. We then apply the method to simulations and experiments of granular compaction. The distribution of global volumes (the volume of the entire packing) is nearly Gaussian and it is difficult to conclude if the theory is valid. On the other hand, the distribution of Voronoï volumes clearly obeys the theoretical prediction.

DOI: 10.1103/PhysRevE.80.031301 PACS number(s): 45.70.Cc, 05.90.+m

I. INTRODUCTION

Edwards and co-workers [1,2] introduced a theory of static granular packings that is closely related to statistical mechanics. This theory rests on three observations: (1) a granular packing is composed of many grains, (2) preparing the packing repeatedly in the same way always yields the same macroscopic state but different microscopic states, and (3) the volume of the packing is the most important macroscopic variable. The first two observations suggest using statistical mechanics and the third motivates replacing the energy U of a thermal system with the volume V of a packing. One can then define the entropy S as the logarithm of the number of states with a given volume. Finally, the compactivity $X=\partial V/\partial S$ is the analog of the temperature. The compactivity is a function of the way the packing is prepared.

This theory was initially met with skepticism. Its formulas were the same as those of the usual statistical mechanics, except for a few letters that were changed. This close resemblance hides some rather profound differences. For example, temperature in statistical mechanics arises when one considers a system in contact with a heat bath. The temperature is independent of the nature of the coupling. In granular statistical mechanics, one might argue that a granular packing is exchanging volume with the rest of the universe, so that the packing is coupled to a "volume bath." But the compactivity depends on how the system is prepared, not on any property of the volume bath. Another problem is that it is quite difficult to test this theory. The entropy function $S(V)$ is difficult to measure and the dependence of X on the parameters of the preparation is unknown.

Nevertheless, it is possible to calculate X from observing density fluctuations. This was first done for granular compaction in a long, narrow tube [3]. The same procedure has been carried out in other experimental situations, such as a granular packing that is periodically fluidized by flowing water [4], or granular compaction in a wide container [5]. Although this method yields X, it does not test the theory of Edwards, for such a calculation is always possible once fluctuations are observed. Nevertheless, experimental work has verified various aspects of the theory, such as the existence of history-independent states [3,4], that can be characterized by density alone [5].

Further work focused on the free volume associated with each particle. The distribution of these volumes is well approximated by a gamma law [6–9] of a form that agrees with the theory of Edwards. These works are probably the strongest evidence supporting the theory.

In this paper, we use a method of testing the theory that has been applied to a spin glass [10] and to the distribution of contact forces [11,12]. This method checks if the volume histograms have the special form. Specifically, the ratio of two overlapping histograms must be an exponential in volume. This is a direct consequence of the Boltzmann-like factor $e^{-V/X}$ present in the theory. This test has the advantage of being generally applicable and of not requiring detailed knowledge of the entropy. On the other hand, the test can yield a "false positive" result when applied to a series of Gaussian distributions with nearly equal variances. We apply this test to data from simulations and experiments of granular compaction. We consider both the total volume of the packing and the Voronoï volumes associated with each particle. In all cases, the observed distributions satisfy the test. The global volume distributions are nearly Gaussian, rendering the interpretation of the results difficult. On the other hand, the distributions of the Voronoï volumes are clearly non-Gaussian and our results are a clear success of the theory.

This paper is organized as follows. In Sec. II, we review some results of statistical mechanics and Edward's theory. This section is necessary to show the difference between the two theories and to pose in detail the questions that this paper addresses. Then in Sec. III, we present our numerical results and in Sec. IV, our experimental ones.

II. CLASSICAL AND GRANULAR STATISTICAL MECHANICS

A. Statistical mechanics of thermal systems

In this section, we present a brief review of classical statistical mechanics. Although this can be found in textbooks, we present it here to support our discussion of the assumptions of granular statistical mechanics.

1. Microcanonical ensemble

The goal of statistical mechanics is to explain how the thermodynamic behavior of macroscopic systems arises from the motion of their microscopic parts. It establishes a connection between macroscopic quantities such as entropy and internal energy and microscopic quantities such as positions and velocities of molecules. This connection rests on Boltzmann's postulate that the entropy is the logarithm of the phase-space volume available to the system

$$S(U) = k_B \ln\left[C(N) \int \delta[U - \mathcal{H}(\mathbf{q})] d\mathbf{q} \right]. \tag{1}$$

Here, S is the entropy and U is the internal energy of a system. The left-hand side of this equation involves therefore only macroscopic quantities that can be determined from the equations of state, for example.

On the right-hand side is a microscopic expression. The Boltzmann constant k_B can be considered as the fundamental unit of entropy. The microscopic degrees of freedom are $\mathbf{q} = (q_1 \cdots q_N)$. It will be assumed that assigning a value to each component of $\mathbf{q}$ completely and uniquely specifies the state of the system. In the following, we consider a classical system where $\mathbf{q}$ contains both the positions and momenta of the particles and take on a continuous range of values. In quantum systems, $\mathbf{q}$ takes on discrete values and the integral becomes a sum. The constant $C(N)$ depends on the number of degrees of freedom and is needed for two reasons. First, the argument of the logarithm must be dimensionless, but the integral over phase space has dimensions. Second, the entropy must be extensive.

The function $\mathcal{H}(\mathbf{q})$, called the Hamiltonian, calculates the energy of any configuration $\mathbf{q}$ of the system. Therefore, the delta function in Eq. (1) selects those configurations compatible with the constraint that the total energy of the system be equal to U. This is appropriate for an isolated system, whose total energy must remain constant.

Now let us consider some other quantity that can be calculated from the system configuration $\mathbf{q}$ by a function $\mathcal{A}(\mathbf{q})$. This quantity will fluctuate as the system changes its configuration. Nevertheless, its average value $\bar{A}$ can be calculated by averaging over all possible configurations, assuming each one to be equally likely

$$\bar{A}(U) = \frac{\int \mathcal{A}(\mathbf{q}) \delta[U - \mathcal{H}(\mathbf{q})] d\mathbf{q}}{\int \delta[U - \mathcal{H}(\mathbf{q})] d\mathbf{q}}. \tag{2}$$

Again, this equation links macroscopic quantities on the left-hand side with microscopic ones on the right-hand side. Note that the denominator is required for normalization and is called the partition function. Using Eq. (1), note that Eq. (2) can be rewritten as

$$\bar{A}(U) = C(N) e^{-S(U)/k_B} \int \mathcal{A}(\mathbf{q}) \delta[U - \mathcal{H}(\mathbf{q})] d\mathbf{q}. \tag{3}$$

This average is called the microcanonical ensemble average.

2. Canonical ensemble

Up to this point, we have assumed that the internal energy U of the system is fixed, corresponding to a completely isolated system. This is not a useful idealization because it is difficult to produce systems to which it applies. It is much more common to observe systems which are held at a constant temperature by exchanging energy with their surroundings. Nevertheless, Eq. (2) can be extended to describe these systems. This is done by dividing the system into a "reservoir" $\mathbb{R}$ and a "small system" $\mathbb{S}$. Each degree of freedom can be assigned to one of these two subsystems: $\mathbf{q} = (\mathbf{q}_R, \mathbf{q}_S)$. We observe only the system $\mathbb{S}$, so that any quantity A that we will want to calculate depends only on $\mathbf{q}_S$. Applying Eq. (2), we obtain

$$\bar{A}(U) = \frac{\int \mathcal{A}(\mathbf{q}_S) \delta[U - \mathcal{H}(\mathbf{q}_S, \mathbf{q}_R)] d\mathbf{q}_S d\mathbf{q}_R}{\int \delta[U - \mathcal{H}(\mathbf{q}_S, \mathbf{q}_R)] d\mathbf{q}_S d\mathbf{q}_R}. \tag{4}$$

Next, we assume that the Hamiltonian can be written as

$$\mathcal{H}(\mathbf{q}) = \mathcal{H}_R(\mathbf{q}_R) + \mathcal{H}_S(\mathbf{q}_S) + \mathcal{H}_{SR}(\mathbf{q}_S, \mathbf{q}_R), \tag{5}$$

with

$$\mathcal{H}_{SR}(\mathbf{q}_S, \mathbf{q}_R) \ll \mathcal{H}_S(\mathbf{q}_S) \ll \mathcal{H}_R(\mathbf{q}_R). \tag{6}$$

We put this form into Eq. (4) and assume that $\mathcal{H}_{SR}$ is so small it can simply be omitted. We obtain

$$\bar{A}(U) = \frac{\int \mathcal{A}(\mathbf{q}_S) \delta[U - \mathcal{H}_S(\mathbf{q}_S) - \mathcal{H}_R(\mathbf{q}_R)] d\mathbf{q}_S d\mathbf{q}_R}{\int \delta[U - \mathcal{H}_S(\mathbf{q_S}) - \mathcal{H}_\mathbf{R}(\mathbf{q_R})] d\mathbf{q}_S d\mathbf{q}_R}. \tag{7}$$

It is now possible to perform the integrals over $\mathbf{q}_R$ because $\mathcal{A}$ depends only on $\mathbf{q}_S$. Equation (1) states that the integrals of the delta functions in Eq. (7) are exponentials of the entropy leading to

$$\bar{A}(U) = \frac{\int \mathcal{A}(\mathbf{q}_S) e^{S_R[U - \mathcal{H}_S(\mathbf{q}_S)]/k_B} d\mathbf{q}_S}{\int e^{S_R[U - \mathcal{H}_S(\mathbf{q}_S)]/k_B} d\mathbf{q}_S}, \tag{8}$$

where $S_R(U_R)$ is the entropy of the reservoir when the reservoir contains energy $U_R = U - \mathcal{H}_S$. Since $\mathcal{H}_S \ll U$, the entropy can be expanded in a Taylor series

$$S_R[U - \mathcal{H}_S(\mathbf{q}_S)] \approx S_R(U) - \left(\frac{\partial S_R}{\partial U} \right) \mathcal{H}_S \approx S_R(U) - \frac{\mathcal{H}_S}{T}, \tag{9}$$

where we have used the thermodynamic identity $T = \partial U / \partial S$. Putting this back into Eq. (8), we have

$$\bar{A}(T) = \frac{\int \mathcal{A}(\mathbf{q}) e^{-\mathcal{H}_S/k_B T} d\mathbf{q}}{Z(T)}, \tag{10}$$

where

$$Z(T) = \int e^{-\mathcal{H}_S/k_B T} d\mathbf{q} \tag{11}$$

is the partition function. Note that we have changed the argument of A from U to T. This is possible because U is an

increasing function of T. We have also dropped the subscript S from the $\mathbf{q}_S$. The average in Eq. (10) is called the canonical ensemble average.

Equation (10) is probably the most-used result in statistical mechanics. We can rewrite it as

$$\bar{A}(T) = \int \mathcal{A}(\mathbf{q})\mathcal{P}_T(\mathbf{q})d\mathbf{q}, \tag{12}$$

where

$$\mathcal{P}_T(\mathbf{q}) = \frac{e^{-\mathcal{H}_S(\mathbf{q})/k_BT}}{Z(T)} \tag{13}$$

is the probability that configuration $\mathbf{q}$ will be realized at temperature T.

3. Fluctuations and probability

Equation (10) predicts the average value $\bar{A}$ a quantity will have at temperature T. If measurements can be made accurately and quickly enough, fluctuations about this mean value will be observed. This is because the system is always changing its configuration, thus causing the measured value of A to change. The probability that A take on a certain value A_0 is

$$p_T(A_0) = \int \delta[A_0 - \mathcal{A}(\mathbf{q})]\mathcal{P}_T(\mathbf{q})d\mathbf{q}. \tag{14}$$

Thus by observing fluctuations of some quantity A, one might be able to learn something about the geometry of phase space. One frequently monitored quantity is the energy U of the subsystem

$$U(T) = \frac{\int \mathcal{H}_S(\mathbf{q})e^{-\mathcal{H}_S/k_BT}d\mathbf{q}}{Z(T)}$$

$$= k_BT^2\frac{\partial}{\partial T}\log Z(T). \tag{15}$$

The second equal sign can be found by differentiating Eq. (11) under the integral sign. Differentiating this relation a second time yields

$$C_V = \frac{\partial U}{\partial T} = \frac{\sigma_U^2}{k_BT^2}, \tag{16}$$

where σ_U^2 is the variance of the distribution of the energy contained in the subsystem. Here, C_V is the specific heat of a thermodynamic system at constant volume. It is the amount of energy that must be added to raise the temperature by one unit.

Let us suppose that we have a thermodynamic system at temperature T_1 and containing energy U_1. Some energy is added so that the internal energy increases to U_2 and the temperature rises to T_2. If we integrate Eq. (16), then we obtain

TABLE I. The analogy between granular packings and thermal systems underlying the theory of Edwards.

Thermal Systems		Granular Systems	
Degrees of Freedom	$\mathbf{q}$	Degrees of Freedom	$\mathbf{q}$
Hamiltonian	$\mathcal{H}(\mathbf{q})$	Volume function	$\mathcal{W}(\mathbf{q})$
Energy	U	Volume	V
Temperature	T	Compactivity	X

$$\frac{1}{k_BT_2} - \frac{1}{k_BT_1} = -\int_{U_1}^{U_2}\frac{dU}{\sigma_U^2}. \tag{17}$$

This equation can be used to determine the temperature if the changes in energy and the fluctuations of the energy are known. This equation is not usually very useful for thermal systems because it is much easier to measure the temperature with a thermometer than to observe fluctuations of energy. It will turn out to be useful, however, for calculating the analog of the temperature in granular packings.

B. Granular statistical mechanics

1. Presentation

The theory of Edwards begins by considering a granular packing prepared in some way. The method of preparation is assumed to be repeatable, so that one could (at least in theory) generate an ensemble of identically prepared packings. This ensemble is then put in analogy with the canonical ensemble. This analogy is summarized in Table I. One replaces the energy U with the volume V of the packing. The Hamiltonian is replaced with the volume function $\mathcal{W}$. After making these changes, Eq. (1) becomes

$$S(V) = \log\int \delta[V - \mathcal{W}(\mathbf{q})]\Theta(\mathbf{q})d\mathbf{q}. \tag{18}$$

The entropy $S(V)$ is the logarithm of the number of ways to arrange the grains that yield a volume V. The function Θ has been added because only certain configurations are stable. If a given configuration $\mathbf{q}$ is unstable (for example, if it contains a grain that floats above the surface without any supporting grains), then $\Theta(\mathbf{q})=0$.

Since we want to use the canonical ensemble, there must be a quantity analogous to the temperature T. This is the compactivity X assumed to be a function of the preparation of the packing. Then, given a quantity A, the probability of observing $A=A_0$ at compactivity X is

$$p_X(A_0) = \int \delta[A_0 - \mathcal{A}(\mathbf{q})]\mathcal{P}_X(\mathbf{q})d\mathbf{q}, \tag{19}$$

in analogy with Eq. (14). The probability that a configuration $\mathbf{q}$ will be realized under the same conditions is

$$\mathcal{P}_X(\mathbf{q}) = \frac{e^{-\mathcal{W}(\mathbf{q})/X}}{Z(X)}\Theta(\mathbf{q}), \tag{20}$$

where the partition function

$$Z(X) = \int e^{-\mathcal{W}(\mathbf{q})/X} \Theta(\mathbf{q}) d\mathbf{q} \tag{21}$$

guarantees that $p_X(\mathbf{q})$ is properly normalized.

2. Discussion

Although the mathematical structure of these two theories is very close, the physics is quite different. For example, Eq. (1) is almost the same as Eq. (18). The entropy in Eq. (1) is the thermodynamic entropy, which can be defined and measured without any reference to a microscopic model, as it was done in the century before Boltzmann. On the other hand, the entropy in Eq. (18) has no such independent existence. It is defined by Eq. (18).

Another important difference is the origin of the exponential in Eq. (13) and in Eq. (20). In Eq. (13), the exponential arises from considering a system in contact with a thermal bath. After making a specific assumption given in Eq. (6), the exponential appears in a mathematical derivation. On the other hand, no such derivation has been proposed for the exponential in Eq. (20). It has simply been inserted, in analogy with Eq. (13). Various qualitative arguments can be suggested, but nothing so precise as the derivation of Eq. (13). The exponential factor in Eq. (20) must therefore be regarded as an assumption of the theory.

In general, the form of $\mathcal{P}_X$ in Eq. (20) is rather special. It can be factored into three parts: a function of X, but not $\mathbf{q}$, a function of $\mathbf{q}$, but not X, and finally an exponential factor where both $\mathbf{q}$ and X appear. Again, there is no known reason why this should be so. One can also ask why $\mathcal{W}(\mathbf{q})$ appears and not some other function of $\mathbf{q}$. Furthermore, X and S are related through the relation $X=\frac{\partial V}{\partial S}$. Note that it is quite easy to construct histograms which do not satisfy these assumptions. An example is given in Sec. II B 4. In the following section, we show how to test these assumptions by examining histograms of volume. Quite surprisingly, they hold for granular compaction.

On the other hand, certain other assumptions given in discussions of granular statistical mechanics cannot be tested by examining the histograms of volume. For example, one often reads that the theory requires that "the forcing assures ergodicity: all mechanically stable configurations must be equally probable and accessible" [4]. A violation of ergodicity has no effect on Eq. (20). If certain stable states were inaccessible, this could be easily incorporated into the definition of $\Theta(\mathbf{q})$. This function already encodes the inaccessibility of mechanically unstable states; adding inaccessible mechanically stable states does not change the structure of the theory. There is also no reason why the stable states must all be equally probable, either. One could use $\Theta(\mathbf{q})$ to weight the more probable states more heavily than the less probable states. Indeed, ergocity can probably not be tested without calculating the integrals over phase space in detail. We do not do this, but simply verify that Eq. (20) has the predicted form, which is already a nontrivial statement.

3. Determination of the entropy and compactivity

We now show how one can test the theory and determine X and S. We first determine X in two different ways. The first way is to use Eq. (17), replacing the thermodynamic quantities with their granular analogs [3–5]

$$\frac{1}{X_2} - \frac{1}{X_1} = -\int_{V_1}^{V_2} \frac{d\bar{V}}{\sigma_V^2(\bar{V})}. \tag{22}$$

In this equation, X_1 and X_2 are two values of the compactivity, corresponding to volumes V_1 and V_2, respectively. σ_V^2 is the variance of the distributions of volume and must be obtained as a function of the expected value $\bar{V}$ of the volume. To apply this equation, one must measure the fluctuations of volume for different packing preparations (i.e., different values of X and V). From this information, one can construct the function $\sigma_V^2(V)$ and integrate the right-hand side of Eq. (22), determining $1/X$ up to an additive constant.

Note that Eq. (22) alone provides no check on the validity of the theory. No matter what the distributions of the volumes were, one could still obtain X by applying Eq. (22). This has limited the interest of previous work that exploits this equation.

However, X can be determined in another way [10–12]. The trick is to obtain $1/X$ from overlapping volume distributions. One simply uses Eq. (19) to obtain the probability $p_X(V)$ of observing a volume V at compactivity X,

$$\begin{aligned} p_X(V) &= \int \delta[V - \mathcal{W}(\mathbf{q})] \left(\frac{e^{-\mathcal{W}(\mathbf{q})/X}}{Z(X)} \right) \Theta(\mathbf{q}) d\mathbf{q} \\ &= \int \delta[V - \mathcal{W}(\mathbf{q})] \left(\frac{e^{-V/X}}{Z(X)} \right) \Theta(\mathbf{q}) d\mathbf{q} \\ &= \frac{e^{-V/X}}{Z(X)} e^{S(V)}. \end{aligned} \tag{23}$$

This result still contains the unknown functions $Z(X)$ and $S(V)$, but suppose we could obtain the same volume V at two different values X_1 and X_2 of the compactivity. Then we could write

$$\frac{p_{X_1}(V)}{p_{X_2}(V)} = \left(\frac{Z(X_2)}{Z(X_1)} \right) e^{V/X_2 - V/X_1}. \tag{24}$$

The ratio of these probabilities is an exponential in V.

This ratio is easy to obtain from experimental or numerical data. One must observe the fluctuations of volume for two different values of X, i.e., for two different ways of preparing the packing. In the case of granular compaction, this means two different strengths of tapping. For each value of X, one then prepares a histogram showing the number of times each value of the volume V was observed. This yields $p_{X_1}(V)$ and $p_{X_2}(V)$. If the histograms overlap enough, the ratio in Eq. (24) can be calculated as a function of V and fitted with an exponential. If the fit turns out to be reasonable, $1/X_2 - 1/X_1$ can be extracted. By comparing many different histograms, $1/X$ can be determined as a function of the method of preparation, up to an additive constant. These results can be compared to those obtained from Eq. (22). If the

histograms do indeed have the form Eq. (23), these two results should agree. This was done in Ref. [10] for a model system.

One can push the analysis a bit further and extract the entropy $S(V)$. Comparing the probability of obtaining two different volumes at the same compactivity yields

$$\frac{p_X(V_1)}{p_X(V_2)} = \frac{e^{-V_1/X}e^{S(V_1)}}{e^{-V_2/X}e^{S(V_2)}}. \tag{25}$$

Taking the logarithm of both sides, we can obtain

$$S(V_2) = S(V_1) + \frac{V_2 - V_1}{X} + \ln p_X(V_2) - \ln p_X(V_1). \tag{26}$$

An alternative way to obtain the entropy is to integrate the relation $X = \partial V / \partial S$,

$$S(V) = \int \frac{1}{X} dV. \tag{27}$$

We thus have two different ways to calculate X and S. To calculate X, we can use either Eq. (22) or (24). If the volume histograms $p_X(V)$ have the form given in Eq. (23), both methods give the same results. However, they are not equivalent, for Eq. (24) works only when $p_X(V)$ have the form predicted by Edward's theory, but Eq. (22) can always be applied. Thus applying Eq. (24) is a test of the theory.

It is also important to realize that both methods determine X only up to an additive constant. Equation (22) contains a definite integral that introduces a constant of integration while Eq. (24) gives the difference in $1/X$ between two different preparations. In this paper, we either arbitrarily fix this constant or adjust it to make X a function of V.

In the same way, we could determine S either from the histograms as in Eq. (26) or the integral in Eq. (27). Again, these methods are not equivalent. Equation (26) relies on the form of $p_X(V)$ where as Eq. (27) does not. Neither are the results necessarily the same, even when $p_X(V)$ has the predicted form. Equation (26) isolates the function $S(V)$ appearing in $p_X(V)$, whereas Eq. (27) relies on the thermodynamiclike identity $X = \partial V / \partial S$. In granular statistical mechanics, there is no reason why the S in the thermodynamiclike relation must be the same as the S appearing in $p_X(V)$. The thermodynamiclike relation was not used in deriving $p_X(V)$ and thus the identification of these two entropies is another supposition of the theory. In contrast, the thermodynamic relation $T = \partial S / \partial U$ is used in deriving the canonical ensemble in thermal statistical mechanics.

It is also important to realize that both methods of calculating S introduce another unknown additive constant. Thus the transformation

$$\frac{1}{X} \to \frac{1}{X} + \beta, \quad S \to S + \beta V + \alpha \tag{28}$$

acts like a "gauge transformation:" applying it does not change the physical observations. However, note that the analogy to the gauge transformation in electromagnetism is only partial. The transformation Eq. (28) does modify $Z(X)$, but this is invisible to our analysis since we do not consider $Z(X)$.

4. Case of generalized gamma distributions

To show that the overlapping histogram test can be a sensitive check of Eq. (24), it is helpful to investigate what would happen if Eq. (23) were not true. Let us consider the case that the volumes are distributed according to a generalized gamma distribution

$$\tilde{p}_X(V) = \frac{\omega_2}{\Gamma\left(\frac{1+\omega_1}{\omega_2}\right)} \lambda^{1+\omega_1} V^{\omega_1} \exp[-(\lambda V)^{\omega_2}], \tag{29}$$

where ω_1 and ω_2 are additional parameters. Note that $\tilde{p}$ has the form of p in Eq. (23) when $\omega_2 = 1$ and $\lambda = 1/X$. We assume λ depends on the preparation of the powder.

Let us now consider what happens when we try to calculate X using the two different methods presented above. Since both λ and X are functions of the preparation, this amounts to calculating X as a function of λ.

Let us consider Eq. (22) first. We must obtain σ_V^2 as a function of the expected value of the volume. The moments of the generalized gamma distribution are

$$\int_0^\infty V^n \tilde{p}(V) dV = \lambda^{-n} \frac{\Gamma\left(\frac{1+n+\omega_1}{\omega_2}\right)}{\Gamma\left(\frac{1+\omega_1}{\omega_2}\right)}. \tag{30}$$

From this relation, one can obtain $\sigma^2(\bar{V})$ and perform the integral in Eq. (22). This yields a relation between X and $\bar{V}$. Equation (30) can be used again to obtain a relation between X and λ,

$$\frac{1}{X_2} - \frac{1}{X_1} = \left[\frac{\Gamma\left(\frac{\omega_1+3}{\omega_2}\right)}{\Gamma\left(\frac{\omega_1+2}{\omega_2}\right)} - \frac{\Gamma\left(\frac{\omega_1+2}{\omega_2}\right)}{\Gamma\left(\frac{\omega_1+1}{\omega_2}\right)} \right]^{-1} (\lambda_2 - \lambda_1). \tag{31}$$

Now let us turn to Eq. (24). The ratio in that equation can be calculated. We do not obtain an exponential in V, except for the case $\omega_2 = 1$. If we fit an exponential to the ratio in some small region around the volume V, we obtain

$$\frac{1}{X_2} - \frac{1}{X_1} = \omega_2 V^{\omega_2 - 1} (\lambda_2^{\omega_2} - \lambda_1^{\omega_2}). \tag{32}$$

Note that Eqs. (31) and (32) agree only when $\omega_2 = 1$, but no restriction is placed on ω_1.

5. Case of overlapping Gaussians

The Gaussian distribution arises frequently whenever systems with a large number of degrees of freedom are considered. It is therefore useful to consider what happens when the method above is applied to overlapping Gaussian distributions. Suppose that the distributions of observed volumes are Gaussians

$$p_{X_1}(V) = \frac{1}{\sigma_1 \sqrt{2\pi}} e^{-(V - \bar{V}_1)^2 / 2\sigma_1^2}, \tag{33}$$

where σ_1^2 is the variance of the distribution and $\bar{V}_1$ is its mean. Suppose we have two Gaussians for $X = X_1, X_2$. The logarithm of the ratio in Eq. (24) is

$$\ln\left(\frac{p_{X_1}(V)}{p_{X_2}(V)}\right) = -\frac{(V-\bar{V}_1)^2}{2\sigma_1^2} + \frac{(V-\bar{V}_2)^2}{2\sigma_2^2} - \ln\sigma_1 + \ln\sigma_2. \tag{34}$$

This function is a parabola, whereas if Eq. (23) holds, we expect a straight line with a slope $1/X_2 - 1/X_1$. Thus, according to Edward's theory, the volume histograms cannot be strictly Gaussian. In many cases, however, the central part of distributions is well approximated by a Gaussian. This is true of gamma distributions [obtained by setting $\omega_2 = 1$ in Eq. (29)]: As the parameter ω_1 increases, so does the range of V where the Gaussian approximation is accurate. This approximation is very good because of the central limit theorem.

The parabola in Eq. (34) resembles a straight line when its curvature is very small. This occurs when the variance of neighboring distributions is nearly the same. Furthermore, we can only determine the ratio in Eq. (34) over a small range of values, where the parabola might be indistinguishable from a straight line. What value of $1/X$ would be found in this case? To find out, consider evaluating the slope of the function in Eq. (34) at $V=(\bar{V}_1+\bar{V}_2)/2$, i.e., midway between the centers of the two distributions. We obtain

$$\frac{1}{X_2} - \frac{1}{X_1} = \frac{1}{2}\left(\frac{1}{\sigma_1^2} + \frac{1}{\sigma_2^2}\right)(\bar{V}_2 - \bar{V}_1). \tag{35}$$

This is a finite difference version of Eq. (22). The two methods thus give the same result. This means that an agreement between Eqs. (22) and (24) is not necessarily significant evidence of Edward's theory. It may simply be the case that we are confronted with Gaussian distributions generated by a completely different process. It is therefore always necessary to check if the data permit a distinction between a Gaussian and distributions arising from statistical mechanics.

C. Application to granular compaction

In this paper, we apply these ideas to granular compaction, where grains are put into a container and subjected to a series of taps. The process has been studied experimentally [3–5] and numerically [13]. One observes that the density approaches a value that depends on the strength and nature of the tapping and then fluctuates around this value. For example, in Fig. 1, we show the dimensionless volume per particle as a function of the number of taps from two simulations of granular compaction. In the lower panel, where the tapping is quite vigorous, the volume fluctuates about a constant value, with the amplitude of the fluctuations also remaining constant. In the upper panel, the tapping is very gentle. After about 20 000 taps, a steady state is (apparently) obtained, but at a smaller volume.

In the following, we examine whether the fluctuations of the granular packing about its long-time average can be considered as thermal fluctuations. We make the hypothesis, therefore, that the fluctuations for $T>20\,000$ in the upper panel of Fig. 1 and for $T>2000$ in the lower panel are sampling the "granular-canonical ensemble" whose states $\mathbf{q}$ are realized with the probability given in Eq. (20).

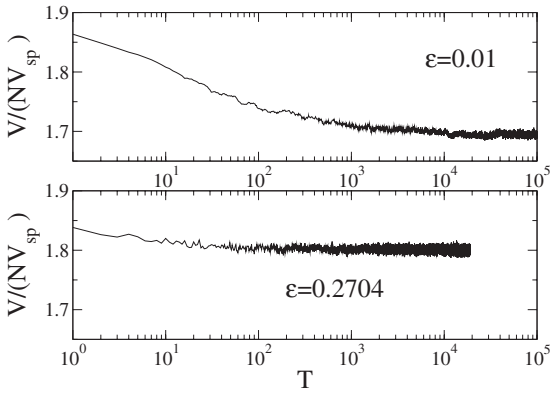

FIG. 1. The volume per particle as a function of the number T of taps for two different values of ε. The volume is given in units of $V_{\rm sp}=\pi D^3/6$, the volume of a single sphere. (Thus the solid fraction is $\nu=NV_{\rm sp}/V$.) In both cases, the size of the periodic domain was $L_x=L_y=16D$, with $N=4096$ particles.

III. NUMERICAL RESULTS

A. Method

We use a numerical model of granular compaction [13] that has been extensively compared to experiments and other numerical models. It has been shown to reproduce many of the macroscopic features of granular compaction, as well as some of the microscopic ones [14,15].

The granular packing is composed of N identical spheres of diameter D contained in a rectangular volume with a flat, solid bottom and periodic boundaries at the sides. The model is entirely geometric; no forces are calculated. First, one models the tap as a dilation of the packing. If z_i is the height of the center of particle i, it is moved to a height $(1+\varepsilon)(z_i - D/2)+D/2$. The diameter D appears in this expression so that the particles resting on the bottom remain there; they are effectively "glued" to the bottom. The parameter ε characterizes the strength of the tap. Examination of the experiments show that ε is proportional to the square of the maximum acceleration experienced during the tap [16].

Once the packing has been dilated, the particles fall back down into place. This is done using a Monte Carlo-like procedure. A small, downward displacement is randomly generated and proposed to a chosen particle. This displacement is generated by first choosing a distance uniformly distributed in $[0,D/10]$. Then an azimuthal angle ϕ is chosen, uniformly distributed in $[0,2\pi]$. Finally, a polar angle is chosen by first drawing a value u from a normal distribution with unit variance and zero mean. If $|u|>1$, another value is drawn until we obtain $|u|\leq 1$. Then, we calculate a polar angle $\theta=\pi(|u|-1)$, where $\theta=-\pi/2$ indicates a movement directly downward. In this way, we are assured that each proposed movement will lower the center of mass of the packing. The proposed movement is rejected if it would cause particles to overlap or penetrate the floor. Otherwise, the movement is accepted and the particle is moved downward. Then another particle is selected and another displacement is generated. This continues until the packing has settled. In the previous implementations of the model, the packing was considered to have finished evolving when the average dis-

placement decreased below a threshold. Here, we wish to compare systems of different sizes, so it is helpful to propose a fixed number of movements to each particle.

One consequence of the movement acceptance criterion is that the particles never touch, even when the packing has settled. A movement that would cause an overlap is rejected and a movement that would cause two particles to touch is generated with a probability zero. Therefore, a settled packing is one where the particle separations have become small. Thus we expect that the densities observed numerically will be smaller than the experimental ones, which is indeed the case.

B. Choice of parameters

The simulation domain has a horizontal size of $L=16D$. We perform simulations with $N=4096$ and $N=8192$ grains, corresponding to $ND^2/L^2=16$ and 32 layers of particles. To check the effect of the horizontal sizes, simulations were done with $L=8D$ and 16 layers of particles ($N=1024$). The results are identical to those obtained with $L=16D$ and 16 layers of particles. Thus we conclude that L has no influence on the results.

The depth of the packing, however, does have an influence on the results. In particular, one must increase the number of proposed moves for deeper packings because the grains at the top of the packing must move farther during the compaction. Accordingly, we use the following formula to calculate the number N_{propose} of moves proposed to each grain after each tap:

$$N_{\text{propose}} = \varepsilon\left(\frac{N}{16L^2} + 0.2\right) \times 10^4. \tag{36}$$

The initial conditions are generated by putting the particles into the periodic domain one after another. First, the horizontal coordinates of the particle are chosen randomly. The sphere is then placed very high above the bed with these coordinates and then lowered until it touches another sphere or the floor. Then the entire packing is submitted to ten taps at $\varepsilon=1$ to mix the particles.

Once the initial condition has been obtained, a large number of simulations at different values of ε was done with $0.01<\varepsilon<1$. This range is much larger than what is experimentally accessible. An analysis of photographs taken during experiments shows dilations corresponding to $\varepsilon<0.1$ [16]. We use a large range of ϵ to test the validity of the theory over a wide range of parameters.

Since the equilibration and correlation times depend on ϵ, the length of the simulation also depends on ε with about $10^4/\varepsilon^{1/2}$ taps being performed. To eliminate transients, we exclude the first 1/3 of each time series from our analysis. To check if an equilibrium has been truly attained, the small simulations ($L=8D$, $N=1024$) were continued for 10 times more taps. These simulations show that small decreases in volume occur for $\varepsilon<0.05$ even after $10^4/\varepsilon^{1/2}$ taps. The decreases are small, however, generally on the order of 1/3 the standard deviation of the distributions of volume. Furthermore, the decrease is slow enough that these simulations can be considered as being in equilibrium, as we will see below.

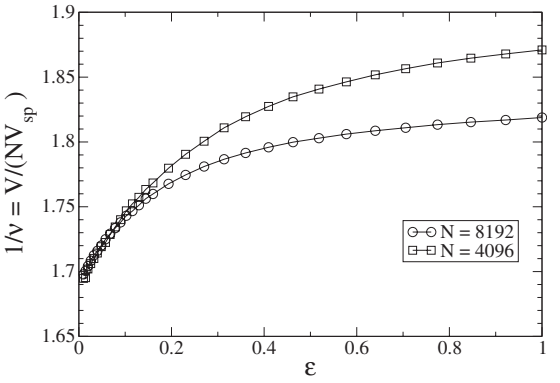

FIG. 2. The inverse solid fraction $1/\nu=V/(NV_{\text{sp}})$ as a function of ε. Here, V is the volume of the packing and $V_{\text{sp}}=\pi D^3/6$, the volume of a single sphere. Data are shown for both the 16-layer packings ($N=4096$) and the 32-layer packings ($N=8192$).

We calculate the volume by dividing the packing into $L_xL_y/(4D^2)$ square vertical columns of size $2D\times 2D$. The height $z_{\max}$ of the highest particle within each column is found and the volume of the packing within the column is then $2D\times 2D\times(z_{\max}+D/2)$. To obtain the volume of the whole packing, one sums the volumes of all the columns. In Fig. 2, we show the volume as a function of ε for both the $N=4096$ and $N=8192$ simulations. To compare these packings of different depths, we compute the inverse packing fraction $1/\nu=V/(NV_{\text{sp}})$, where $V_{\text{sp}}=\pi D^3/6$ is the volume of a single sphere. The densities of the two depths coincide for $\varepsilon<0.2$, but the deeper sample is denser for $\varepsilon>0.2$.

Examination of vertical solid fraction profiles $\nu(z)$ shows that the density is not constant with height, as it is in the experiment. For small ε, density decreases with height, and for large ε, it increases. The relationship between the density profile, the number of moves proposed to each particle, and the method of choosing the particles to move is a complicated issue [17]. It should also be noted that a curious behavior has recently been noted for $\varepsilon>1$: the average volume becomes nonmonotonic [15]. Thus the curves in Fig. 2 would exhibit a maximum if larger values of ε were probed. In this paper, we will not consider these issues further, but simply investigate whether the systems can be considered to be sampling a granular-canonical average according to Eq. (20).

C. Calculation of compactivity

The volume is calculated after each tap, permitting us to construct histograms of volume for each value of ε. Several examples are shown in Fig. 3. These volume histograms are obtained by binning the volumes observed in the last 2/3 of each time series, giving an estimate of $p_{X(\varepsilon)}(V)$. Specifically, the range of volumes is divided up into n small intervals of size ΔV ($\Delta V=D^3$ in Fig. 3). Then, the number of points N_i that fall into each interval i is counted. The probability density p_i within the interval i is thus

$$p_i = \frac{N_i}{N_{\text{total}}\Delta V}, \tag{37}$$

where N_{total} is the total number of points in all the intervals. This gives a probability density whose integral over all val-

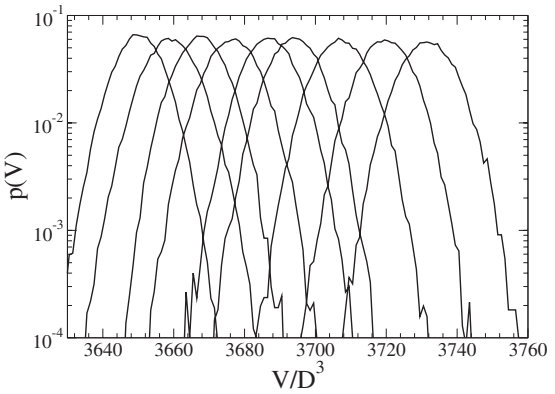

FIG. 3. Histograms of the volume V for $\sqrt{\varepsilon}$ ranging from 0.14 to 0.30 with steps of 0.02 for $N=8192$. The most probable value of V increases monotonically with ε. To eliminate transients associated with the approach to the equilibrium, only volumes in the last 2/3 of the simulations were used.

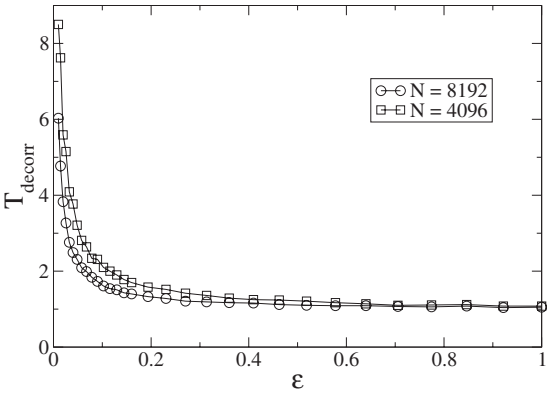

FIG. 4. The decorrelation time T_{decorr}, defined in Eq. (38). This decorrelation time used to estimate the number of independent points in each bin of the histogram, thus determining the uncertainty of the probability p_i.

ues of V is unity, as required. The histograms obtained in this way are nearly Gaussian as one can quickly see by looking at Fig. 3, where they have a clear parabolic shape when plotted logarithmically. We must therefore consider the possibility (discussed in Sec. II B 5) that the apparent success of the statistical-mechanical theory be due to the limited range of accessible volumes.

Next, the uncertainty of this probability must be calculated. This requires determining the number of independent points in each bin. Note that each measurement is not independent, since each volume measured is correlated with the volume measured at the previous tap. We estimate a decorrelation time T_{decorr} from the autocorrelation function $C(T)$ of the volume. Specifically, T_{decorr} solves

$$\int_0^{T_{\text{decorr}}} [1 - C(T)]dT = 1. \tag{38}$$

In our case, recall that time is discrete, but application of this equation requires continuous time. We solve this problem by declaring that $C(T)$ takes on the value of the autocorrelation function for the smallest integer greater than T. Thus for $0 < T \leq 1$, $C(T)=C(1)$. Thus T in Eq. (38) is the time, nondimensionalized using the temporal separation of the taps. If $C(1)=0$, then $T_{\text{decorr}}=1$ and the volumes at successive taps are completely independent, so that the number of independent taps is equal to the number of taps. As T_{decorr} increases, the number of independent taps decreases. The obtained decorrelation times are shown in Fig. 4. Not surprisingly, one has $T_{\text{decorr}} \approx 1$ for large ε and T_{decorr} increases as the tapping becomes gentler.

Once the decorrelation time T_{decorr} has been obtained, one can determine the number of independent points in interval i as N_i/T_{decorr}. Thus, we estimate the uncertainty of the probability as

$$\Delta p_i = \frac{\sqrt{N_i T_{\text{decorr}}}}{T_{\text{end}} \Delta V}. \tag{39}$$

In order to apply Eq. (24), we need to obtain the probability of observing a certain volume for different values of ε. This is quite easy to do, as shown in Fig. 3. The histograms overlap substantially, meaning that the ratio in Eq. (24) can be calculated for a large number of points. We thus plot logarithmically the ratio of the probabilities. Some examples are shown in Fig. 5. One obtains straight lines, as predicted by Eq. (24).

Fits such as those in Fig. 5 were performed for every pair of vibrations $(\varepsilon_1, \varepsilon_2)$ where there are at least ten points to fit. One can check the quality of the fit by calculating its χ^2 statistic

$$\chi^2 = \sum_{i=1}^{n} \frac{(y(x_i) - y_i)^2}{\Delta y_i^2}, \tag{40}$$

where (x_i, y_i) are the observed points, x_i being the independent variable, and y_i the dependent one. The uncertainty of the measurement is given by Δy_i and the function $y(x)$ is the theoretical prediction being tested. The sum is taken over all the observed points. If χ^2 is of order of the number n of fitted

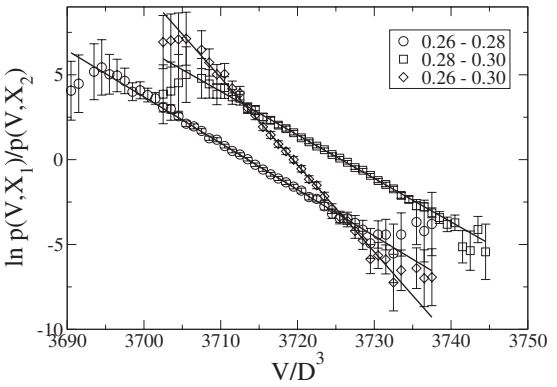

FIG. 5. Logarithmic graph of the ratio shown in Eq. (24), obtained from the histograms of Fig. 3. As predicted, one obtains an exponential in volume, except at the tails of the distribution. The numbers in the legend give the values of $\varepsilon^{1/2}$ used to generate X_1 and X_2. These data are taken from the $N=4096$ simulations.

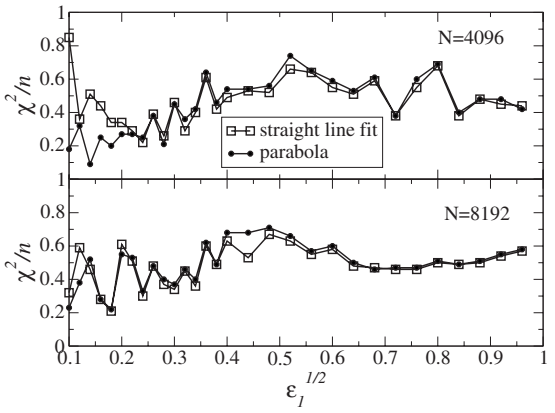

FIG. 6. Comparison of the χ^2 statistic for the linear fit (squares) and the parabolas (circles). For clarity, only fits arising from neighboring pairs of histograms $[(\varepsilon_1,\varepsilon_2)=(0.1,0.12),(0.12,0.14),\ldots]$ are shown.

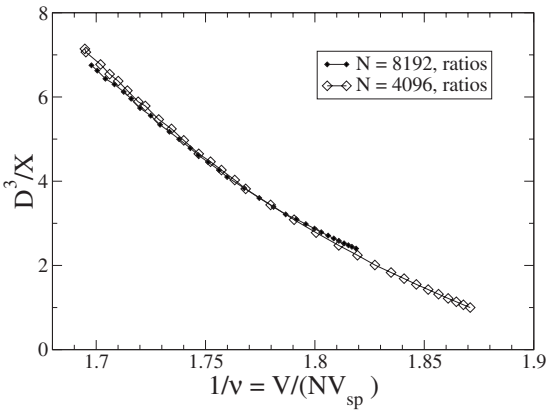

FIG. 7. Compactivity X as a function of the inverse solid fraction $1/\nu=V/(NV_{\mathrm{sp}})$, where $V_{\mathrm{sp}}=\pi D^3/6$ is the volume of a single grain. The additive constant β in Eq. (28) has been adjusted here so that the two curves lie nearly on top of one another: $\beta_{8192}-\beta_{4096}=1.5$.

points, then the fit is reasonable. A large value of χ^2/n indicates that the points cannot be fitted to a straight line. The largest value of χ^2/n encountered is just less than 1.6, meaning that all the pairs of histograms that overlap significantly conform to Eq. (24) to within statistical uncertainty.

To obtain these high-quality fits, it is necessary to incorporate the decorrelation time into the uncertainty, as done in Eq. (39). Furthermore, if transients are not eliminated, they contaminate the distribution so that Eq. (24) does not hold. Simulations with small ϵ are particularly affected by this problem, since the approach to equilibrium is slow when the tapping is weak. As mentioned above, eliminating the first 1/3 of each time series is enough to solve this problem.

However, we must consider the alternative explanation of the straight lines in Fig. 5. Perhaps the straight lines appearing there are simply small sections of the parabolas predicted in Eq. (34). To this end, we compute the ratio in Eq. (34) for each pair of overlapping histograms. We do this by simply taking the mean and the variance of the two histograms. This enables us to calculate the coefficients of the parabola in Eq. (34). This parabola can then be compared to the data by calculating its χ^2 statistic and comparing it to that of the linear fit. This is done in Fig. 6, where we show the χ^2 statistic for both the linear fit and the parabolic curve calculated from the mean and variance of the two contributing histograms. The χ^2 statistics are nearly identical, with the exception of $\varepsilon^{1/2}<0.2(\varepsilon<0.04)$ for the small $(N=4096)$ systems. Thus, our data neither confirms nor contradicts the statistical-mechanical theory. The histograms that we observe may be the central parts of distributions that conform to Eq. (23) or they may be Gaussians generated by some other process.

Nevertheless, one can continue obstinately with the analysis and calculate $1/X$ as a function of ε. Equations (22) and (24) yield equivalent results, as anticipated for the case of nearly Gaussian distributions. One finds that the results depend on N as well as ε. However, ε is not a good parameter because the results of the simulation depend on many other parameters, such as the number of moves proposed to each particle. It is therefore not clear that $\varepsilon=0.1$ has the same meaning for the two different system sizes. We therefore plot $1/X$ as a function of the inverse solid fraction $1/\nu=V/(NV_{\mathrm{sp}})$, where V_{sp} is the volume of a single grain. The dependence on N can then be eliminated if one chooses the constant β in Eq. (28) appropriately. The results of doing this are shown in Fig. 7. As expected, X decreases as the density increases.

What does it mean that $1/X$ is independent of N? In Eq. (22), we see that $1/X_2-1/X_1\propto(V_2-V_1)/\sigma_v^2$. This quantity must remain constant as N changes. Since $V\propto N$, we must have $\sigma_V\propto N^{1/2}$. This is precisely the scaling predicted by the central limit theorem. Thus the global density is behaving like a sum of many independent, identically distributed random variables.

A careful examination of the curves in Fig. 7 indicates that they do not exactly coincide. Their slopes are slightly different. This may be due to the influence of the boundaries, which is more important in the smaller sample. In conclusion, the distributions of the global packing volumes are consistent with the form predicted by Edward's theory, Eq. (23), but we are unable to distinguish them from simple Gaussian distributions.

D. Statistics of volume around individual particles

1. Description of data

Although Edward's theory was originally proposed for the total volume of a packing, the focus of much recent work has been on the distribution of volumes associated with each particle [6–9]. The total volume of the packing is partitioned into regions, each region being associated with a particle. The most common method is to construct Voronoï cells and that is the method used here.

We use the $L_x=L_y=16D$ simulations with $N=8192$ particles. The depth of these packings is approximately $32D$. We write the particle positions to a file every 1000 taps and then calculate the Voronoï volumes associated with each particle. Only those volumes recorded during the last 2/3 of the simulation are used, so that local and global analyses are based on the same configurations.

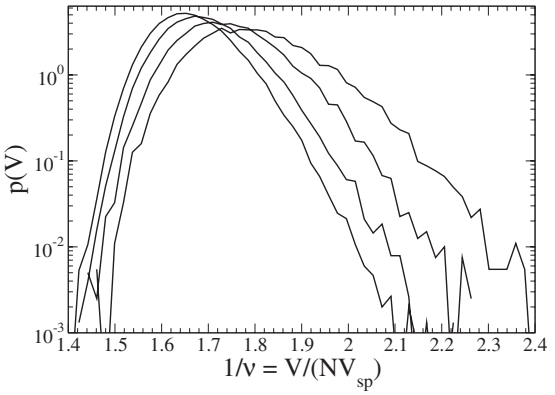

FIG. 8. Examples of histograms for the volumes associated with each particle. These histograms are for the grains found in the slice $10<z/D<15$ with $\varepsilon=0.01,0.04,0.1444,0.7744$.

Inspection of the data shows that the density depends on height and therefore the distribution of volumes must also depend on the height. We therefore divide the packing into horizontal slices of thickness $5D$ and construct the histograms of the Voronoï volumes for each slice and each value of ε. Voronoï cells are considered as members of the same population if their centers are in the same slice with the same value of ε, even when appearing at different times. Figure 8 shows some histograms obtained in this way. The resulting distributions are clearly asymmetric and therefore non-Gaussian.

Since all distributions overlap significantly, it is possible to check Eq. (24) for every possible pair of $(\varepsilon_1,\varepsilon_2)$ belonging to the same slice. Some statistics concerning the results are shown in Table II. First of all, it is clear that the linear fit based on Eq. (22) describes the data much more accurately than the assumption of overlapping Gaussians. Furthermore, the fits are better in the middle of the packing than at the top and bottom. This is probably due to boundary effects [17]. In the center of the packing, the distribution of volumes is well described by a function of the form given in Eq. (23). In the following, we therefore neglect the top and bottom layers of the packing.

TABLE II. The maximum and mean χ^2 statistic for the linear and Gaussian fits at different levels in the packing. Recall that all pairs of $(\varepsilon_1,\varepsilon_2)$ have been calculated and taken into account. The values for linear fit arises from a straight-line fit of the ratio in Eq. (24) and the Gaussian values result from assuming the volume histograms are Gaussians as in Eq. (34).

	Linear fit		Gaussian	
Slice	Maximum	Mean	Maximum	Mean
$0<z/D<5$	4.7	1.5	31.2	11.4
$5<z/D<10$	2.8	0.7	61.3	17.3
$10<z/D<15$	1.2	0.6	45.7	10.2
$15<z/D<20$	1.2	0.5	21.0	4.9
$20<z/D<25$	1.4	0.6	13.2	2.9
$25<z/D<30$	2.8	0.8	9.2	2.1

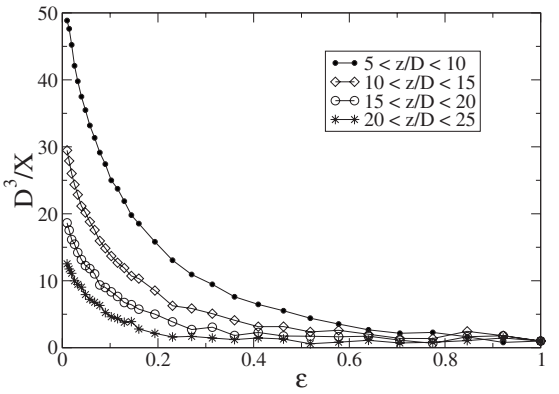

FIG. 9. Compactivity in different parts of the pile.

2. Compactivity and entropy

Since the distributions of volume have the form predicted by the statistical-mechanical theory, it is meaningful to calculate X. In Fig. 9, we show X as a function of ε. Note that X varies within the packing. The compactivity decreases as one descends toward the bottom. As the tapping becomes weaker, the X decreases, as was observed for the global measure of the volume. But the value of X deduced from the Voronoï volumes is smaller than the value obtained for packing as a whole (compare Figs. 7 and 9).

Earlier work [5] showed that the compactivity was a function of the density. We can check if this holds true at the microscopic level by calculating the average volume $\langle V\rangle$ in each slice and for each value of ε and then plotting X as a function of $\langle V\rangle$. If one plots $1/X$ using the compactivities shown in Fig. 9, the points for the different slices fall on parallel curves. But $1/X$ has been determined only up to an additive constant, which has been assumed to be the same for all slices in Fig. 9. If we adjust this constant, assigning a different constant to each slice, one can collapse all the curves together, as shown in Fig. 10. Thus the variation of X with height is solely due to the variation of density.

In Fig. 11, we show the entropy for one slice in the middle of the packing. It is calculated using two different ways: either by integrating $\partial S/\partial V=1/X$ or by using Eq. (25). Both

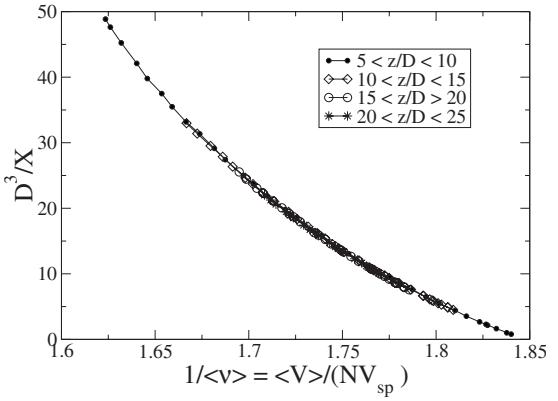

FIG. 10. Inverse compactivity as a function of the average volume. The additive constant β in Eq. (28) has been adjusted so that the curves lie on top of one another.

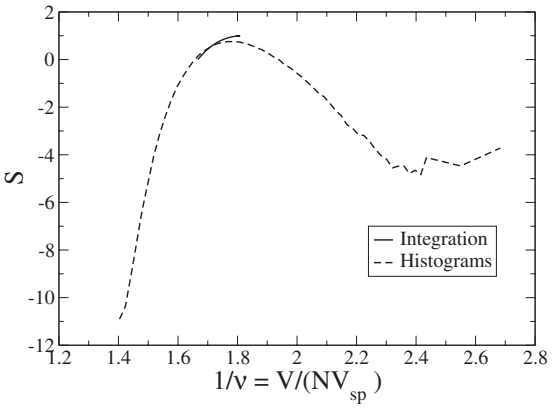

FIG. 11. Entropy calculated by integrating $\partial S/\partial V=1/X$ or from Eq. (25) for the Voronoï volumes in the middle of the packing.

of these ways determine S up to an additive constant α, so that the negative values in Fig. 11 are simply a consequence of the choice of this constant. Note that the two methods are not equivalent. Equation (25) allows one to calculate the entropy over a much wider range of volumes. All that is needed to calculate $S(V)$ is that the volume V be represented in a histogram and that the distributions of volumes be well described by Eq. (23). On the other hand, calculating $S(V)$ by integrating $1/X$ requires that V be equal to the average volume for some value of X.

Another point to note is that the two methods yield different values of $\partial S/\partial V$. The line labeled "Histograms" in Fig. 11 is the function $S(V)$ in Eq. (23), but its derivative with respect to V is not equal to $1/X$ that appears in the Boltzmann-like factor $e^{-V/X}$. This difference cannot be removed by adjusting β because the same value of β was used by both methods.

Finally, note the presence of a density with maximum entropy. Such a maximum has been observed before in different models related to granular compaction [18,19]. It is expected from physical considerations. At low densities, we expect a low entropy because there are many constraints on the way the particles are to be placed. At high densities, stable states are rare, so again the number of available arrangements is low. Between these two extremes, the entropy must be large, as it is in Fig. 11. Nevertheless, one should be cautious in interpreting Fig. 11 for changing the arbitrary additive constant β can shift the location of the maximum or even eliminate it. Furthermore, the number of points at large volumes is relatively small.

Thus, the Voronoï volumes obey certain aspects of Edward's theory, but not all. The exponential factor in the density histograms is present, but the compactivity is different from that calculated for the entire packing. This differs from the behavior of thermal systems, where the same temperature governs both the total energy and the individual degrees of freedom. This means that the individual Voronoï volumes sum up to the packing volume in a different way than the energies of the various degrees of freedom add up to the total energy.

Recent work suggests that the correct microscopic degrees of freedom are not Voronoï volumes, but "quadrons" [20]. This is because the number of quadrons in a granular packing is equal to the number of independent line segments needed to draw the network that connects the centers of touching grains. This suggests that quadrons are the correct variables for a microscopic description of granular packings.

3. Gamma distribution

Aste and Di Matteo studied [9] the distributions of Voronoï volumes in a wide variety of situations. They found that all the data can be fitted with a gamma distribution

$$p(V)=\frac{k^k}{\Gamma(k)}\frac{(V-V_{\min})^{k-1}}{(\bar{V}-V_{\min})^k}\exp\left(-k\frac{V-V_{\min}}{\bar{V}-V_{\min}}\right). \quad (41)$$

Here, k is a parameter, with $k\approx 12$ for disordered jammed states, and $V_{\min}$ is the minimum volume possible. Are our data consistent with this distribution? Equation (41) can be written in the form of Eq. (23) if k and $V_{\min}$ are considered as constants, independent of the preparation (and thus independent of X). The preparation therefore enters into Eq. (41) only through the mean density $\bar{V}$. This is consistent with our observation that the compactivity depends only on the local average volume, i.e., $\bar{V}$.

Putting Eq. (41) into the form of Eq. (23) gives the following expressions:

$$X=\frac{k}{\bar{V}-V_{\min}}, \quad S(V)=(k-1)\ln(V-V_{\min}). \quad (42)$$

If this expression for the compactivity X holds, then the curve in Fig. 10 should be a straight line with a slope of k. This curve is not straight and its slope of order 100. The entropy in Fig. 11 looks much different from the predicted logarithm, but one could increase the arbitrary constant β in Eq. (28) to remove the maximum. The resulting curve would look similar to a logarithm.

In conclusion, the result of Aste and Di Matteo can be cast in the form predicted by Edward's theory, Eq. (23), but the values of X and S so obtained do not agree with our data. It may be that our procedure yields packings quite different from theirs. It would be necessary to apply the overlapping histogram test to their data to obtain a definite answer to this question.

IV. EXPERIMENTAL RESULTS

A. Experimental setup

The experimental setup has already been described elsewhere [5,21]. It consists in $d=1$ mm diameter glass spheres placed in a glass cylinder of diameter $L\approx 10$ cm. The cylinder containing the grains is tapped vertically at regular intervals ($\Delta t=1$ s). Each tap is controlled by an entire cycle of a sine wave at a fixed frequency $f=30$ Hz: $V(t)=V_{\mathrm{MAX}}[1-\cos(2\pi ft)]/2$ for $0<t<1/f$ and $V(t)=0$ elsewhere. This applied voltage is connected to an electromagnetic exciter (LDS V404) which induces a vertical displacement to a moving part supporting the container and the beads. The resulting motion of the whole system is monitored by an accelerometer at the bottom of the container. This motion is more com-

TABLE III. Experimental results. We show both the solid fraction and the inverse solid fraction $1/\nu=\bar{V}/(NV_{sp})$ used to calculate the compactivity.

Γ	N	$1/\nu=\bar{V}/(NV_{sp})$	$\nu=NV_{sp}/\bar{V}$
3.15	2001	1.6327 ± 0.0063	0.6125
4.20	2962	1.6387 ± 0.0064	0.6102
5.25	1416	1.6431 ± 0.0061	0.6086
6.30	1923	1.6468 ± 0.0066	0.6072

plicated than a simple sine wave: at first, the system undergoes a positive acceleration followed by a negative acceleration with a minimum equal to $-\gamma_{max}$. After the applied voltage stops, the system relaxes to its normal position. When γ_{max} is large enough, the bead packing takes off from the bottom of the container and achieves a flight until it crashes back to the bottom. The control parameter is the tapping intensity $\Gamma=\gamma_{max}/g$, where $g=9.81$ m s^{-2}. The packing fraction is measured using a γ-ray absorption setup [5,21]. It is deduced from the transmission ratio of the horizontal collimated γ beam through the packing $T=A/A_0$, where A and A_0 are, respectively, the activities counted on the detector with and without the presence of the granular medium. From the Beer-Lambert law for absorption, we can derive an estimation of the volume fraction in the probe zone $\rho\approx-(\mu L)^{-1}\ln(T)$, where μ is the absorption coefficient of the beads. The collimated γ beam is nearly cylindrical with a diameter of 10 mm and intercepts perpendicularly the vertical axis of the vessel. We use an acquisition time of 60 s for each measure which leads to a precision of 0.003. The packing fraction of the sample is estimated from the ratio T averaged on approximately 7 cm height from the bottom of the cylinder. Packing fraction profile measurements report a constant packing fraction along the vertical axis.

B. Results

Several time series at different values of Γ were carried out. The results are summarized in Table III. As described above, one measures the solid fraction ν of the packing, which is proportional to the inverse volume. In this section, we calculate volume as simply $V/(NV_{sp})=1/\nu$. The number of points is lower than in the numerical case because it is much more difficult to obtain the experimental data.

Figure 12 shows the histograms obtained from the data. Their form is nearly Gaussian, although a slight asymmetry is sometimes visible. Note that the experimental volumes are smaller than the numerical ones. The largest volume in Fig. 12 is about $1/\nu=1.67$, less than the smallest volume $1/\nu=1.69$ in Fig. 7. Furthermore, the range of volumes observed is much smaller than in the numerical results. The variation in the mean value $1.639\leq\bar{V}\leq1.653$ is just a bit less than 1% of the volume. In comparison, the range of volumes observed numerically is 10% of the volume (see Fig. 2). The variation of volume observed microscopically (Fig. 11) is even greater.

Figure 13 shows one example of the ratio in Eq. (24), together with the straight-line fit predicted by that equation,

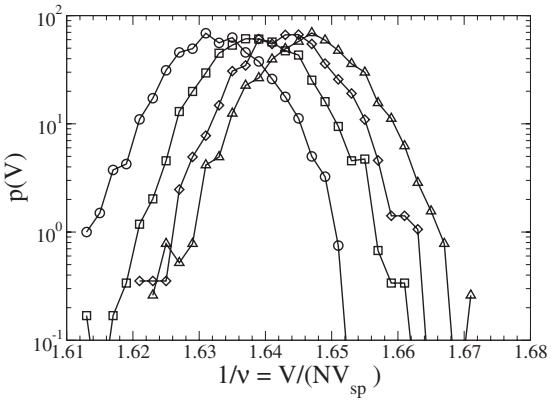

FIG. 12. Histograms of volume obtained from the experiments. The curves are for $\Gamma=3.15$ (circles), 4.20 (squares), 5.25 (diamonds), and 6.30 (triangles). See Table III.

as well as the values that arise from assuming the histograms are Gaussians. As one can see, the results are not decisive, although the Gaussian assumption fits the data slightly better. The other pairs of histograms yield data where the difference between the two theories is even smaller. Therefore, our experimental results do not permit us to confirm the statistical-mechanical theory.

Nevertheless, we can extract $1/X$ from fits such as those in Fig. 13. The results are shown in Fig. 14. The arbitrary constant β has been chosen so that $1/X=1$ for the largest value of X.

Let us now compare the experimental results of Fig. 14 to the numerical ones in Fig. 7. The graphs cannot simply be placed on top of one another because the ranges of $1/X$ and $1/\nu$ both differ. Let us consider the difference in $1/X$ first for this is the most dramatic. In Fig. 7, $1\leq1/X<8$, whereas the range of $1/X$ in Fig. 14 is at least 50 times greater: $1\leq1/X<400$. As stated above, there is an arbitrary constant involved in our calculations of $1/X$, but that does not help reconcile this last result. The slopes of the lines are radically

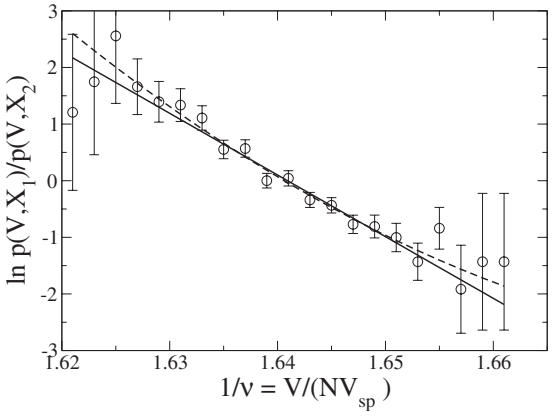

FIG. 13. Logarithmic graph of the ratio shown in Eq. (24), obtained from the histograms of Fig. 12, for the histograms $\Gamma=4.20$ and $\Gamma=5.25$. Also shown are the possible fits. Solid curve: straight-line fit used to extract $1/X$; for this fit, $\chi^2/n=0.6143$. Dashed line: curve obtained by assuming histograms are Gaussians; $\chi^2/n=0.4941$.

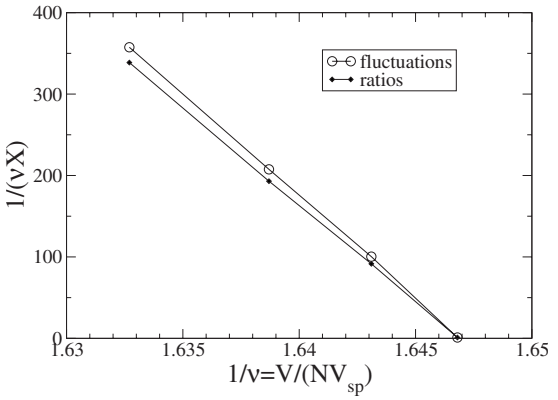

FIG. 14. $1/X$ observed in the experiments. The arbitrary constant β has been chosen so that $1/X=1$ for the largest value of Γ. The line labeled "fluctuations" was obtained with Eq. (22) and the one labeled "ratios" from Eq. (24).

different. In Fig. 7, the slope of the line is about -30 ($1/X$ decreases by about 3 between $1/\nu=1.75$ and $1/\nu=1.85$), whereas in Fig. 14, the slope is -25000 ($1/X$ decreases by about 250 between $1/\nu=1.635$ and $1/\nu=1.735$).

But the units of $1/X$ in the two figures are not the same. Recall that the values of $1/X$ are the slopes of the lines in Figs. 5 and 13 and the x axes of these figures are not the same. In Fig. 5, volume is measured in units of V/D^3 whereas $V/(NV_{\rm sp})$ is used in Fig. 13. Thus the values of $1/X$ from Fig. 13 must be divided by $NV_{\rm sp}/D^3=\pi N/6$. Assuming a packing of about 10 cm, there are about $N=10^6$ grains in the experiment. Thus the slope of the line in Fig. 14 needs to be divided by roughly 5×10^5 before being compared to Fig. 7. This yields experimental values of $1/X$ that are about 1/500 of the numerical ones.

There are two factors that could account for this difference. First of all, the accuracy of the density measurement is 0.3%, as stated in Sec. IV A. This seems quite accurate, but the range of observed densities is quite small: the mean volumes are spread over less than 1% (see Table III) and the width of the histograms is about 2.5%. Thus the experimental uncertainty can significantly broaden the width of the histograms. This reduces the slopes in Fig. 13, leading to an increase in $1/X$.

A second factor that may explain the gap is that the effective value of N is less than the total number of particles. When the density is measured, a beam of gamma-rays traverses the cylindrical sample. As this occurs, the sample is simultaneously rotated and raised, so that one obtains an average over the whole sample. But grains near the top and the bottom are excluded from measurement and, furthermore, particles near the center are weighted more strongly than those at the edges because the beam always passes through the center, but only occasionally through a given grain near the edge. A related difference is that the numerical volumes correspond to a fixed number of particles, whereas experimentally, one measures the number of particles found in a fixed volume.

Although these two factors might reduce the gap between experiment and simulation, they seem unlikely to account for the entire difference. This indicates that the numerical model and the simulation have significant quantitative differences. This is confirmed if one examines the x axes of Figs. 7 and 14: these figures concern nonoverlapping intervals of density.

V. CONCLUSION

We have applied the test first proposed by Dean and Lefèvre [10] of Edward's statistical mechanics of powders. This test checks that the histograms of volume have the predicted form $p_X(V)=e^{S(V)}e^{-V/X}/Z(X)$. A consequence of this form is that the ratio of two overlapping histograms must be an exponential in V. Furthermore, the compactivity X can be extracted from this ratio. We extended this analysis by showing how to extract the entropy $S(V)$ over a wide range of volumes.

We applied this test to granular compaction using both numerical and experimental data. In all cases we examined, the test indicated that theory is valid: the ratio of any two sufficiently overlapping histograms could indeed be fitted to an exponential. However, the test can yield a false positive when the volume histograms are Gaussians with nearly equal variances. In this case, the ratio of the histograms cannot be distinguished from an exponential if the range of observed volumes is too small. For this reason, our results concerning the total volume of the packing are inconclusive. Our data do not permit us to say whether the statistical-mechanical theory applies or whether the volume distributions are Gaussians of a very different origin.

On the other hand, our results for the Voronoï volumes associated with each grain were more conclusive. The distribution of these volumes was clearly non-Gaussian and the histograms have the form predicted by the Edward's theory. We calculated the compactivity X from these histograms and found that it depended only on the local density. The entropy was also calculated: it exhibits a maximum, although one must be cautious when interpreting these results.

We believe that this test of Edward's theory is promising because it can be applied in many situations and does not rely on obtaining an analytic expression of the volume histograms. Nevertheless, care must be taken to eliminate a false positive result arising from Gaussian distributions. Furthermore, the test does not confirm the microscopic details of Edward's theory, such as the probability a given state be realized depends only on its volume.

ACKNOWLEDGMENTS

We thank the Institut für Computerphysik at the University of Stuttgart for computer time. We acknowledge funding from the French Ministry of Education and Research (ACI énergie et conception durable ECD035—Verres de grains).

[1] S. F. Edwards and R. B. S. Oakeshott, Physica A **157**, 1080 (1989).
[2] S. F. Edwards and D. V. Grinev, Phys. Rev. E **58**, 4758 (1998).
[3] E. R. Nowak, J. B. Knight, E. Ben-Naim, H. M. Jaeger, and S. R. Nagel, Phys. Rev. E **57**, 1971 (1998).
[4] M. Schröter, D. I. Goldman, and H. L. Swinney, Phys. Rev. E **71** 030301 (2005).
[5] Ph. Ribière, P. Richard, P. Philippe, D. Bideau, and R. Delannay, Eur. Phys. J. E **22**, 249 (2007).
[6] F. da Cruz, F. Lechenault, and O. Dauchot, in *Powders and Grains 2005*, edited by R. García-Rojo, H. J. Herrmann, and S. McNamara (Taylor & Francis, London, 2005).
[7] F. Lechenault, F. da Cruz, O. Dauchot, and E. Bertin, J. Stat. Mech.: Theory Exp. (2006) P07009.
[8] T. Aste, T. Di Matteo, M. Saadatfar, T. J. Senden, M. Schröter, and H. L. Swinney, Europhys. Lett. **79**, 24003 (2007).
[9] T. Aste and T. Di Matteo, Phys. Rev. E **77**, 021309 (2008).
[10] D. S. Dean and A. Lefèvre, Phys. Rev. Lett. **90**, 198301 (2003).
[11] S. Henkes, C. S. O'Hern, and B. Chakraborty, Phys. Rev. Lett. **99**, 038002 (2007).
[12] S. Henkes and B. Chakraborty, Phys. Rev. E **79**, 061301 (2009).
[13] P. Philippe and D. Bideau, Phys. Rev. E **63**, 051304 (2001).
[14] P. Ribière, P. Richard, R. Delannay, D. Bideau, M. Toiya, and W. Losert, Phys. Rev. Lett. **95**, 268001 (2005).
[15] L. A. Pugnaloni, M. Mizrahi, C. M. Carlevaro, and F. Vericat, Phys. Rev. E **78**, 051305 (2008).
[16] P. Ribière, Ph.D. thesis, Université de Rennes 1, 2005.
[17] S. Kiesgen de Richter, G. Le Caër, and R. Delannay, Europhys. Lett. **85**, 58004 (2009).
[18] D. S. Dean, Eur. Phys. J. B **15**, 493 (2000).
[19] J. J. Brey and A. Prados, Powder Technol. **182**, 272 (2008).
[20] G. Frenkel, R. Blumenfeld, Z. Grof, and P. R. King, Phys. Rev. E **77**, 041304 (2008).
[21] P. Philippe and D. Bideau, Europhys. Lett. **60**, 677 (2002).